Journal of Catalysis 283 (2011) 168–177

Contents lists available at SciVerse ScienceDirect

Journal of Catalysis

journal homepage: www.elsevier.com/locate/jcat

Core/shell-structured Al-MWW@B-MWW zeolites for shape-selective toluene disproportionation to *para*-xylene

Yong-Jun Ji, Bin Zhang, Le Xu, Haihong Wu *, Honggen Peng, Li Chen, Yueming Liu, Peng Wu *

Shanghai Key Laboratory of Green Chemistry and Chemical Processes, Department of Chemistry, East China Normal University, North Zhongshan Rd. 3663, Shanghai 200062, PR China

ARTICLE INFO

Article history:
Received 3 June 2011
Revised 10 August 2011
Accepted 11 August 2011
Available online 23 September 2011

Keywords:
Core/shell zeolite composite
MCM-22
Borosilicate
Disproportionation of toluene
Shape-selective catalysis
para-Xylene

ABSTRACT

A shape-selective core/shell-structured Al-MWW@B-MWW composite catalyst has been hydrothermally synthesized through isomorphically overgrowing borosilicate on premade MCM-22 aluminosilicate. The secondary growth of borosilicate enlarged obviously the thickness of the platelet crystallites of MCM-22 and increased the surface Si/Al ratio from 16 to 222. The Fourier transform infrared (FTIR) spectra of adsorbed 2,6-di-*tert*-butylpyridine indicated that the Brønsted acid sites located on the external surface were virtually covered completely by the generated B-MWW layer, whereas those acid sites within channels were still accessible and detectable by using pyridine or ammonia as probing molecules. When applied to the disproportionation of toluene on a fixed-bed reactor, the Al-MWW@B-MWW composite catalysts exhibited significantly enhanced *para*-xylene selectivity in comparison with normal MCM-22 and its physical mixture with B-MWW. Al-MWW@B-MWW's unique catalytic behaviors were ascribed to an effective suppression of *para*-xylene isomerization as a result of removal of non-shape-selective acid sites on the external surface.

1. Introduction

para-Xylene is one of the most important aromatics widely used as the raw material of polyethylene terephthalate and polyester. The selective production of *p*-xylene via disproportionation of toluene or alkylation of toluene with methanol has attracted intensive studies by using various solid acid catalysts of zeolites including ZSM-5 [1–6], mordenite [7], Beta [8,9], X [10], and Y zeolites [11–13]. The possibility of employing mesoporous Al-MCM-41 as *p*-xylene production catalyst was also investigated [14]. Among them, ZSM-5 is of particular interests because the MFI topology possesses the 10-membered ring (MR) channels with a pore size very comparable to the molecular dimension of benzene or *p*-xylene. A unique shape selectivity *p*-xylene is thus expectable through modifying ZSM-5 properly. The *para*-selectivity is usually decreased significantly by the side reactions like isomerization of *p*-xylene which is favored by the acid sites on the external surface [15]. Hence, to obtain high *para*-selectivity, it is necessary to remove or poison the acidic sites on the external surface. In last decades, many modification techniques have been developed to enhance effectively the *para*-selectivity of ZSM-5, including impregnation of phosphorous, MgO, or boron [1,2], precoking [16,17], chemical vapor deposition (CVD) [18,19], or chemical liquid deposition (CLD) of silica [6,20,21]. Although a significant improvement in *para*-selectivity has been achieved by impregnation of inorganic oxides, an obvious decrease in catalytic activity is inevitable. The precoking modification is often difficult to control and needs to be repeated after the recovered zeolite catalysts are regenerated by calcination. SiO_2-CVD or SiO_2-CLD modification with simple silicon alkoxides, i.e., tetraethyl orthosilicate (TEOS), is then employed to improve *para*-selectivity through laborious and complicated processes.

Zeolite MCM-22, a novel aluminosilicate with the MWW topology [22], is structurally close to aluminosilicates PSH-3 [23] and SSZ-25 [24], borosilicate ERB-1 [25], and silicalite ITQ-1 [26]. Deriving from a lamellar precursor, MCM-22 possesses an unusual crystalline structure consisting of two independent non-intersecting 10-MR channel systems, one of which contains large 12-MR supercages with an inner free space of $0.71 \times 0.71 \times 1.82$ nm. Moreover, it possesses 12-MR half cups on the external surface. The unique structure, high thermal stability, and large surface area make MCM-22 be useful catalysts in a variety of reactions. The acid sites located in 10-MR channels and 12-MR supercages play significant role in selective production of ethyl benzene and cumene [27–30]. With respect to selective formation of *p*-xylene, Zhu et al. reported that the 10-MR channels were possible to give a high conversion and a high *para*-selectivity in toluene methylation [31]. We once demonstrated that MCM-22 is essentially a shape-selective catalyst in the disproportionation of toluene [32]. Its supercages serve as open reaction spaces for accommodating bulky intermediate of toluene disproportionation, which is favorable for the reaction at a relatively low temperature of 573 K. On the other

* Corresponding authors. Fax: +86 21 6223 2292 (P. Wu).
E-mail addresses: hhwu@chem.ecnu.edu.cn (H. Wu), pwu@chem.ecnu.edu.cn (P. Wu).

0021-9517/$ - see front matter © 2011 Elsevier Inc. All rights reserved.
doi:10.1016/j.jcat.2011.08.007

hand, the 10-MR windows are benefit for restricting the formation of *ortho*- and *meta*-xylene. Nevertheless, the *para*-selectivity was decreased as a result of isomerization of *p*-xylene. It is possible to enhance the *para*-selectivity by removing the external surface acid sites via selective dealumination or poisoning with large amine molecules [32,33]. New modification methods are still expected to produce selectively *p*-xylene by taking the advantage of MWW structure.

Recently, core/shell composite zeolites have been paid many attentions due to their synergistic performance in catalytic reactions [34–38]. The *para*-selectivity is possibly improved by synthesizing core/shell composite materials with an active zeolite core and an inactive outer zeolite shell, in which the acidic properties of the external surface of zeolites are altered [39–45]. These composites allow better adsorption or diffusion of molecules within zeolite crystallites in comparison with conventional materials modified by oxide deposition. Nishiyama et al. synthesized a composite of H-ZSM-5 coated with polycrystalline silicalite-1 layer via repeated hydrothermal synthesis and showed that the silicalite coating increased the *para*-selectivity up to 99.9% in the alkylation of toluene with methanol [41,42]. MCM-22/MCM-41 composite synthesized by overgrowing MCM-41 mesosilica over the crystal surface of MCM-22 was also shown to be *para*-selective in the alkylation of toluene with dimethyl carbonate [46].

It is still a challenging work to improve the shape selectivity of MCM-22 (Al-MWW) through removal of its external surface acid sites by isomorphic overgrowth of a non-acidic silicalite shell. This is because hydrothermal crystallization of MWW-type silicalite (ITQ-1) requiring a dual templating system lacks controllability [47]. Making use of corresponding borosilicate (B-MWW) with an extremely weak acidity but having more available and controllable synthesis routes, we have taken an alternative way in this study to design shape-selective catalysts through overgrowing borosilicate on MCM-22 crystallites. The resulting Al-MWW@B-MWW composite exhibited a highly improved *para*-selectivity in toluene disproportionation. After investigating in detail the relationship between acidity and catalytic performance, particularly in correlation to enhanced *para*-selectivity, we demonstrated that covering the external Brønsted acid sites with B-MWW layer was of a great contribution.

2. Experimental

2.1. Material preparation

Following previously reported procedures [22], aluminosilicate MCM-22, denoted as Al-MWW, was hydrothermally synthesized from deionized water, colloidal silica (30 wt.% SiO_2), sodium aluminate (40.52 wt.% Na_2O, 53.52 wt.% Al_2O_3), sodium hydroxide (96 wt.%), and hexamethyleneimine (HMI, >98 wt.%) as structure-directing agent (SDA). The gel with the molar composition of $1.0SiO_2/0.025Al_2O_3/0.05Na_2O/0.35HMI/20H_2O$ was crystallized in a Teflon-line autoclave under rotation (100 rpm) at 423 K for 5 days. On the other hand, borosilicate B-MCM-22 (B-MWW) was synthesized by modifying the procedures for ERB-1 [25], using piperidine (PI) as SDA in fluoride media. The crystallization was carried out at a molar ratio of $1.0SiO_2/1.33H_3BO_3/1.4PI/0.5HF/20H_2O$ and at 443 K for 5 days. The system was a basic media since the amount of PI used was far in excess of that of HF. After cooling down the autoclave, the solid products were gathered by filtration, washed with deionized water, and dried at 353 K overnight.

Al-MWW@B-MWW core/shell materials were synthesized by adding a desirable amount of premade Al-MWW precursor into the gel mentioned in B-MWW synthesis but at the beginning in the absence of colloidal silica and HF. The mixture was subjected to ultrasonic treatment for 0.5 h to make Al-MWW particles highly dispersed in a homogenized suspension. Colloidal silica sol and HF (40 wt.%) were then added dropwise into the mixture under continuous stirring. After mechanically stirred for another hour, the thick gel was crystallized at 443 K for 4 h–5 days. The resulting solid product was collected by filtration, washed thoroughly with deionized water, and dried at 353 K overnight. The synthesis was carried out by fixing the SiO_2 amount in colloidal silica at 3.0 g, while varying amount of Al-MWW added. The samples thus prepared are denoted as Al-MWW@B-MWW(x), where x represents the weight of Al-MWW added. For control experiment, a physical mixture of Al-MWW and B-MWW was prepared by mixing two zeolites at a weight ratio of 1:2. The sample is denoted as Al-MWW/B-MWW. All samples were calcined in air at 823 K for 10 h to remove the organic species occluded. They were then ion-exchanged with 1 M NH_4Cl solution for three times at 353 K for 2 h. The zeolites were converted into proton form by calcination in air at 823 K for 6 h.

2.2. Catalyst characterizations

The catalysts were characterized by various techniques. X-ray diffraction (XRD) patterns were recorded on a Rigaku Ultima IV X-ray diffractometer (35 kV and 25 mA) using Cu Kα radiation (λ = 1.5405 Å). N_2 adsorption was carried out at 77 K on a BELSORP-MAX instrument after outgassing the samples for 10 h under vacuum at 573 K. The crystal morphology and size were measured by scanning electron microscopy (SEM) on a Hitachi S-4800 microscope. Transmission electron microscopy (TEM) images were collected on a JEM-2100 microscope operating at an accelerating voltage of 200 kV. The samples were ground, dispersed in ethanol, and deposited on the copper grids prior to observation. X-ray photoelectron spectroscopy (XPS) measurements were taken on ESCALAB 250 (VG) using Al Kα ($h\nu$ = 1486.6 eV) radiation. The amount of Si, Al, and B was quantified by inductively coupled plasma (ICP) on a Thermo IRIS Intrepid II XSP atomic emission spectrometer after dissolving the samples in HF solution. Acidity was measured by temperature-programmed desorption of ammonia (NH_3-TPD) with a Micromeritics tp-5080 equipment equipped with a thermal conductivity detector (TCD) detector. Typically, 100 mg of sample was pretreated in helium stream (30 mL min^{-1}) at 823 K for 1 h. The adsorption of NH_3 was carried out at 323 K for 1 h. The catalyst was flushed with helium at 373 K for 2 h to remove physisorbed NH_3 from the catalyst surface. The TPD profile was recorded at a heating rate of 10 K min^{-1} from 373 K to 823 K. IR spectra were collected on a Nicolet NEXUS-FTIR-670 spectrometer at room temperature. A self-supported wafer (50 mg and Ø 2 cm) was set in a quartz IR cell sealed with CaF_2 windows, where it was evacuated at 673 K for 2 h before the pyridine adsorption. The adsorption was carried out by exposing the wafer to a pyridine vapor (1.3 kPa) at room temperature for 0.5 h. The physisorbed pyridine was then removed by evacuation at 423 K for 1 h. Similarly, the IR spectra were measured using 2,6-di-*tert*-butylpyridine as probe molecule to measure the surface acidity of zeolites [48,49].

2.3. Catalytic reactions

Toluene disproportionation, 1,3,5-triisopropyl benzene (TIPB) cracking and *p*-xylene isomerization were all performed using a continuous flow system in a fixed-bed quartz reactor (i.d. 15 mm). The reactions were carried out under atmospheric pressure using nitrogen as a carrier gas. The catalyst was activated at 773 K in nitrogen flow (30 mL min^{-1}) for 1.5 h before the reaction. The reactant was fed into the reactor at a rate of 1.7 mL h^{-1}. The typical catalyst loading, flow rate of nitrogen carrier, and reaction temperature were 0.2 g, 30 mL min^{-1}, and 573 K, respectively. This

corresponded to a weight hourly space velocity (WHSV) of 7.36 h^{-1} for toluene. To investigate the effect of contact time on toluene disproportionation, the amount of catalyst was varied in the range of 0.01–0.35 g. In poisoning experiments, 2,4-dimethylquinoline (DMQ) was co-fed continuously at a rate of 100 μL min^{-1} into the reactor together with toluene or 1,3,5-TIPB. The liquid products were collected periodically with an ice/water cold trap at 273 K and analyzed on a gas chromatograph (Shimadzu 14B, flame ionization detector, FFAP capillary column).

3. Results and discussion

3.1. Preparation and characterizations of Al-MWW@B-MWW core/shell materials

Fig. 1 shows the XRD patterns of as-synthesized Al-MWW, B-MWW, and Al-MWW@B-MWW composites with Al-MWW weight varying from 1.5 g to 3 g. The samples showed that the reflections were characteristic of the MWW-type lamellar precursor at 2θ = 2–10°, which are assigned to [001], [002], [100], [101], and [102] planes [22]. The diffractograms also fully agreed with the published patterns at higher angels and were free of the reflections other than MWW structure. All patterns were very comparable in intensity, indicating that the samples were highly crystalline materials. Comparing with those of Al-MWW (Fig. 1a), the reflections of B-MWW and Al-MWW@B-MWW shifted to higher angles (Fig. 1b–f). This difference was observed more obviously for the [3 1 0] reflection. In the case of the borosilicate-containing materials, the unit cell parameters shrank as a function of incorporating boron ions into the zeolite framework. This was very similar to [B]-ZSM-5 which showed a significant lattice contraction in comparison with [Al]-ZSM-5 [50]. The observed phenomena evidenced the isomorphous substitution of boron atoms with a smaller ionic radius than Al and Si ions. The shorter B–O bond length would reduce the unit cell volume for B-containing materials. After the samples were calcined to remove the organic species at 823 K for 10 h, the layer-related [0 0 1] and [0 0 2] reflections almost disappeared or shifted to higher angles as a result of interlayer condensation (XRD patterns not shown). The specific surface area and pore volume of calcined Al-MWW@B-MWW samples, measured from N_2 adsorption isotherms at 77 K, were in the same range as Al-MWW, B-MWW, and their mixture (Table 1), confirming that they were porous zeolites with a high crystallinity.

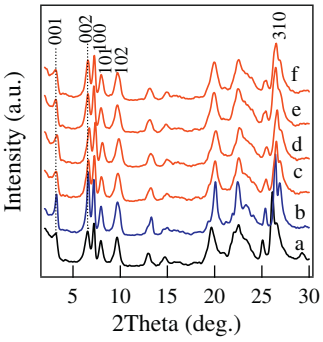

Fig. 1. XRD patterns of as-synthesized Al-MWW (a), B-MWW (b), Al-MWW@B-MWW(1.5 g) (c), Al-MWW@B-MWW(2 g) (d), Al-MWW@B-MWW(2.5 g) (e), and Al-MWW@B-MWW(3 g) (f).

The preconditions for forming the aimed core/shell structure in Al-MWW@B-MWW were that the premade Al-MWW crystallites were not destroyed or dissolved in basic media during hydrothermal process, but served as scaffolds for overgrowing borosilicate shell. We have thus traced the crystallization process to check whether the Al-MWW crystallites disappeared especially at initial stage. Fig. 2 shows the XRD patterns of Al-MWW@B-MWW(1.5 g) as-synthesized at 443 K for a different period of time and corresponding crystallization curve. The mixture of crystalline Al-MWW and amorphous gel consisting of boron and silicon showed already the characteristic reflections due to the MWW topology even before secondary crystallization (0 h) (Fig. 2A, a), although relatively low in intensity. The MWW structure-derived diffraction peaks increased in intensity during whole process. The sample crystallinity was estimated from the [0 0 2], [1 0 0], [1 0 1], [1 0 2], and [3 1 0] reflections. Showing a typical "S" type curve, the crystallization process increased the crystallinity continuously with prolonging time. The crystallinity was almost leveled off after 24 h (Fig. 2B). The results assumed that the Al-MWW crystallites at least were not dissolved to serve as crystallization seeds in the synthetic system. The overgrowth of MWW borosilicate was carried out in the fluoride media which was free of alkali cations and employed secondary amine (PI) with a relatively weak basicity as the SDA rather than using quaternary ammonium hydroxide. This would be helpful to make the Al-MWW crystallites intact.

The fact that the Al-MWW crystallites were well preserved in synthesis did not ensure the overgrowth of borosilicate really on their surface. The SEM images were thus measured to investigate the crystallite morphology and size. Fig. 3 shows the images of Al-MWW and Al-MWW@B-MWW composite materials. The samples all appeared to be fully crystalline materials free of impurities other than MWW phase. Al-MWW exhibited a morphology of thin platelets with an average thickness of about 20 nm (Fig. 3A). Different from the MFI zeolites with changeable morphology depending on the synthesis conditions, the MWW zeolites always show nearly the same platelet morphology irrespective of greatly different gel compositions with various heteroatoms (Al, Ti, or B) or different SDA (PI or HMI). This raised difficulty in recognizing whether the core/shell structure was really constructed. Nevertheless, when fixing the amount of silica to 3 g in secondary synthesis gels while varying the amount of premade Al-MWW from 3.0 g to 1.5 g, we

Table 1
Physicochemical properties of various MWW-type zeolites.

Samples	Crystallite thickness[a] (nm)	Si/Al ratio		Si/B ratio		SSA[d] (m^2 g^{-1})	PV[d] (cm^3 g^{-1})
		Bulk[b]	Surface[c]	Bulk[b]	Surface[c]		
Al-MWW	20	22	16	–	–	569	0.379
B-MWW	40	–	–	12.6	10	514	0.349
Al-MWW @B-MWW(1.5 g)	50	64	222	14	8.2	522	0.361
Al-MWW/B-MWW	20–40	65	28	16	23	519	0.352

[a] Average thickness estimated from SEM images.
[b] Determined by ICP.
[c] Determined by XPS.
[d] Specific surface area (SSA, Langmuir) and pore volume (PV) both measured by N_2 adsorption at 77 K.

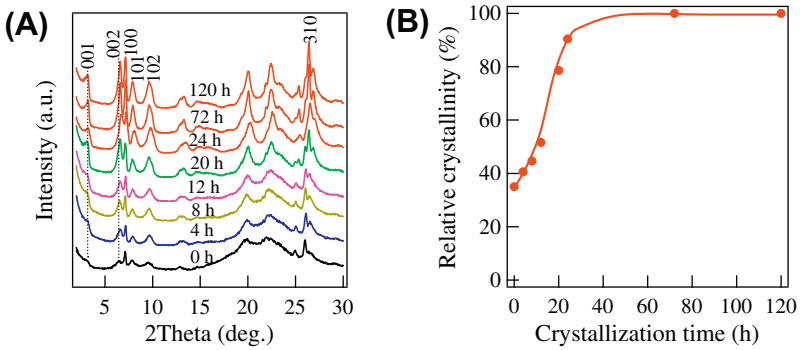

Fig. 2. XRD patterns of Al-MWW@B-MWW(1.5 g) as-synthesized at 443 K for a different period of time (A) and crystallization curve (B).

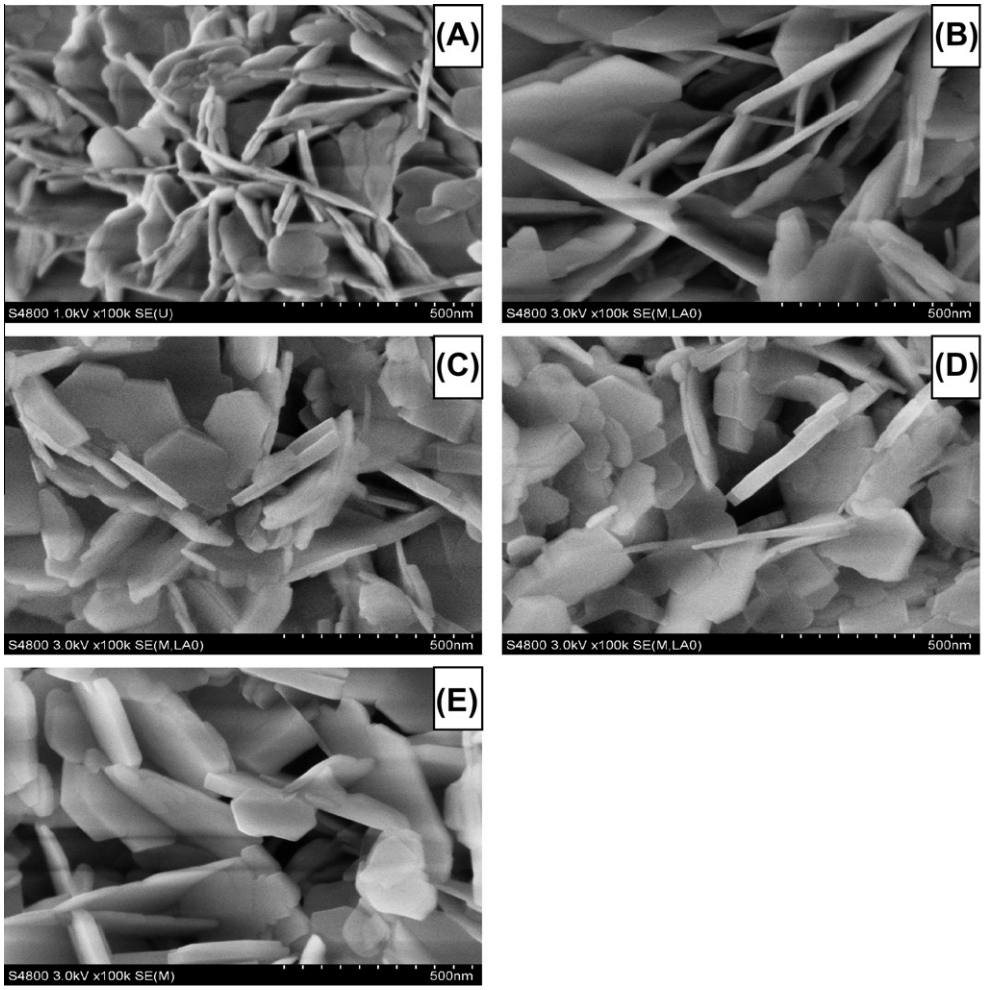

Fig. 3. SEM images of Al-MWW (A), Al-MWW@B-MWW(3 g) (B), Al-MWW@B-MWW(2.5 g) (C), Al-MWW@B-MWW(2 g) (D), and Al-MWW@B-MWW(1.5 g) (E).

found the platelet thickness increased systematically (Fig. 3B–E). When the added amount of Al-MWW was decreased to 1.5 g, the thickness was enlarged remarkably and reached about 50 nm (Table 1).

The dimension of the Al-MWW and Al-MWW@B-MWW(1.5 g) crystallites was further investigated with transmission electron microscopy (TEM). As shown in Fig. 4, the Al-MWW@B-MWW sample did not show any contrast difference because of isomorphic overgrowth of the zeolite with the same topology. Nevertheless, in agreement with the SEM images, the TEM images showed that Al-MWW@B-MWW possessed an enlarged platelet thickness in comparison with original Al-MWW. These results verified that B-MWW was grown on the surface of Al-MWW crystallites successfully, probably leading to a core/shell-structured composite.

The changes of surface chemical compositions after secondary overgrowth of zeolite different in chemical composition would provide further information about the presence of core/shell structure. Fig. 5 showed the Al 2p and B 1s XPS spectra of Al-MWW, Al-MWW/B-MWW, Al-MWW@B-MWW(1.5 g), and B-MWW. As a

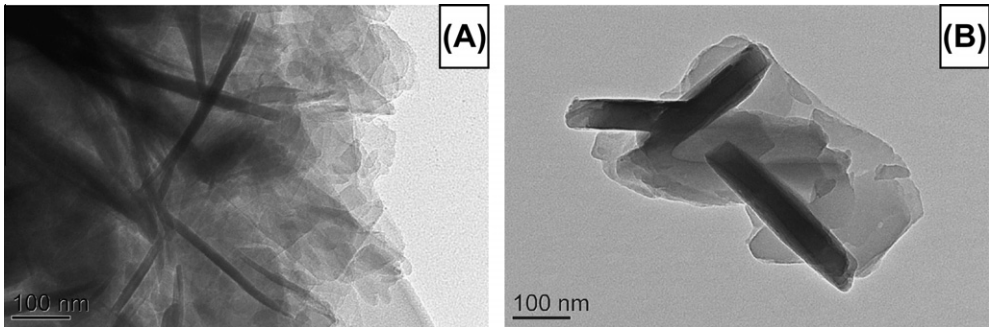

Fig. 4. TEM images of Al-MWW (A) and Al-MWW@B-MWW(1.5 g) (B).

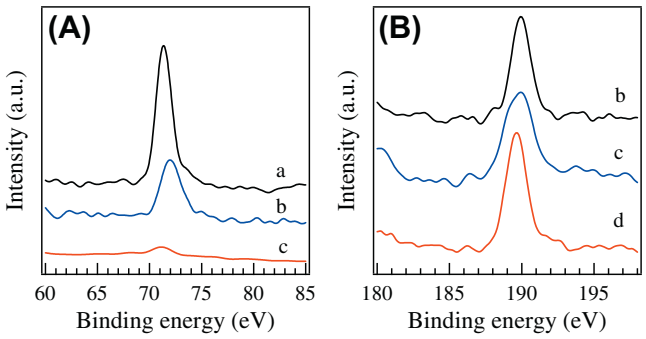

Fig. 5. Al 2p (A) and B 1s (B) XPS spectra of Al-MWW (a), Al-MWW/B-MWW (b), Al-MWW@B-MWW(1.5 g) (c), and B-MWW (d).

pure aluminosilicate, Al-MWW reasonably showed the most intensive Al 2p peak (Fig. 5A, a). When it was physically mixed with B-MWW, the dilution lowered the peak intensity obviously for Al-MWW/B-MWW (Fig. 5A, b). The Al-MWW@B-MWW sample showed an extremely weak Al 2p peak (Fig. 5A, c), implying that the aluminosilicate crystallites were covered by borosilicate rather than coexisted simply as a mixture. On the other hand, both Al-MWW@B-MWW and Al-MWW/B-MWW showed very intensive B 1s peaks, which were even comparable to pure borosilicate B-MWW (Fig. 5B, b–d). The surface Si/Al and Si/B ratios determined by XPS characterization were summarized together with the bulk ratios given by ICP analysis in Table 1. The bulk ratios and the surface ratios (Si/Al and Si/B) both increased for Al-MWW/B-MWW in comparison with those of Al-MWW and B-MWW. This is simply due to diluting effect for physical mixtures. Al-MWW/B-MWW had a surface Si/Al ratio of 28 and a surface Si/B ratio of 23 (Table 1), indicating that Al and B elements were detectable simultaneously on the crystallite surface. On the other hand, the surface ratios of Al-MWW@B-MWW were 222 and 8.5, respectively. However, the bulk ratios were almost the same as those of Al-MWW/B-MWW. Thus, the crystallites of Al-MWW@B-MWW were highly Al-deficient but slightly abundant of B on crystallite surface. The results can be taken as clear evidences for the presence of aimed core/shell structure in Al-MWW@B-MWW.

Fig. 6 shows the results of energy dispersive X-ray microanalysis (EDS) line scanning along the edge of platelet crystallite of Al-MWW@B-MWW. Both B and Al were detected, but obviously, there were a large number of B elements but less Al element on the crystallite surface. The EDS investigation qualitatively verified again that Al-MWW was covered by the B-MWW layer generated in secondary synthesis. The above-mentioned comprehensive characterizations supported that Al-MWW@BMWW possessed a core/shell structure with secondary crystallized B-MWW covering the premade Al-MWW crystallites, and it was a highly crystalline porous material.

3.2. Acidic properties of Al-MWW@B-MWW

The acidic properties of core/shell MWW zeolite were first characterized using NH_3-TPD technique. Fig. 7 compares its profiles with that of Al-MWW, B-MWW, and Al-MWW/B-MWW. B-MWW showed only one desorption peak around 470 K, while the other three samples showed one more desorption peak centered at 690 K. The former is assumed to physically adsorbed ammonia and/or those adsorbed on weak acid sites, whereas the latter is the contribution of the ammonia adsorbed on strong acid sites [51]. Similar to other borosilicates such as MFI-type B-ZSM-5 [50], B-MWW was essentially of non-acidic or only contained extremely weak acid sites, possibly due to the Si–OH–B bridging hydroxyls with a much weaker acidity than Si–OH–Al. With the largest amount of aluminum, Al-MWW showed an intensive

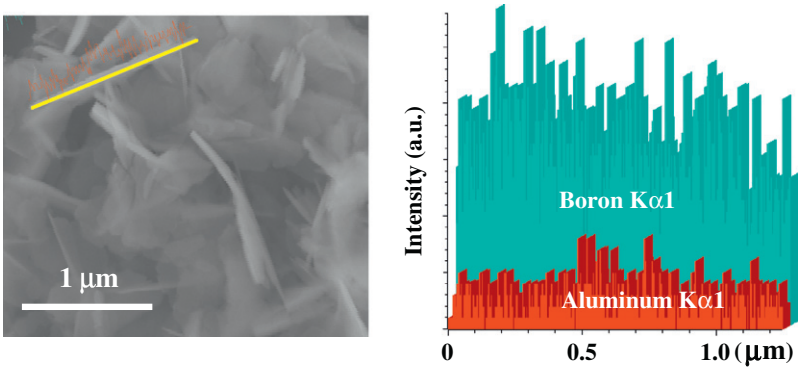

Fig. 6. EDS line scanning of Al-MWW@B-MWW(1.5 g).

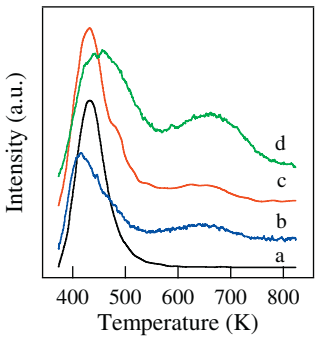

Fig. 7. NH_3-TPD profiles of B-MWW (a), Al-MWW@B-MWW(1.5 g) (b), Al-MWW/B-MWW (c), and Al-MWW (d).

ammonia desorption at 690 K corresponding to strong acid sites. Compared with Al-MWW, Al-MWW/B-MWW and Al-MWW@B-MWW composite had a smaller desorption amount of ammonia corresponding to the strong acid sites and showed almost the same maximum temperature of desorption (Fig. 7b–d). Thus, incorporation of B-MWW decreased the amount of strong acid sites as a result of diluting effect either by physical mixing or by secondary crystallization, but it altered little the acid strength of the framework Al in Al-MWW. B-MWW existing as a mixture or a shell phase on Al-MWW crystallites may have some contribution to the weak acid sites as the ammonia desorption at 470 K was observed obviously for Al-MWW/B-MWW and Al-MWW@B-MWW (Fig. 7b and c). Thus, containing a smaller amount of Al-related acid sites, Al-MWW@B-MWW was still characteristic of a strong acidity as Al-MWW.

The acid properties were further examined by FTIR spectroscopy using pyridine adsorption (Py-IR) technique. The samples in proton form were pretreated under evacuation at 673 K and were then adsorbed with pyridine vapor at 423 K. Fig. 8 shows the spectra in the region of pyridine ring vibrations after removal of physisorbed pyridine molecules. Three main absorption bands could be observed at about 1544, 1490, and 1450 cm^{-1} for all samples. The 1544 cm^{-1} band is assigned to the vibration of pyridine molecules adsorbed on Brønsted acid sites, while the bands around 1450 cm^{-1} are due to Lewis acid sites-related and/or hydrogen-bonded pyridine [52,53]. On the other hand, the pyridine molecules adsorbed on both Brønsted and Lewis acid sites contribute to the 1490 cm^{-1} band [52]. The baseline went upward for three B-containing materials in the region of over 1500 cm^{-1} (Fig. 8b–d), which is because of the appearance of Si–O–B stretching vibration around 1400 cm^{-1} [54]. In the case of B-MWW, the pyridine-related bands nearly disappeared after pyridine desorption at 523 K (Fig. S2d). This was consistent with the results of MFI-type borosilicate [50], indicating that the acid strength of the framework B in B-MWW was very weak. For other three Al-MWW-containing zeolites, the pyridine-related bands, in particular the 1545 cm^{-1} band, still remained and decreased only slightly after the desorption at 523 K (Fig. S2a–c), implying the existence of strong Brønsted acid sites. The results also verified that the strong Brønsted acid sites in Al-MWW@B-MWW were mainly contributed by Al-MWW rather than by B-MWW. However, the amount of Brønsted acid sites in Al-MWW/B-MWW and Al-MWW@B-MWW was much lower than that of pure Al-MWW because of lower Al contents. The results agreed with above NH_3-TPD investigation, verifying that Al-MWW@B-MWW contained a strong Brønsted acidity but with a lower amount than Al-MWW.

NH_3–TPD profiles and Py-IR spectra consistently showed that Al-MWW@B-MWW was essentially the same as Al-MWW in acid strength but contained less strong acid sites due to dilution by B-MWW. As ammonia and pyridine are relatively small probing molecules, they would provide information mainly about the bulk acidity of zeolites. It is preferred to employ bulky amine as prober to study the changes in surface acidity following overgrowth of B-MWW with a weak acidity on Al-MWW crystallites.

2,6-Di-tert-butyl-pyridine (2,6-DTBPy), with a too large molecular dimension to penetrate through the micropores of zeolites, is reported to be chemisorbed only on the external acid sites [48]. DTBPy-IR spectra are thus useful for evaluating the Brønsted acidity on the surface of zeolite crystallites. Fig. 9 shows the spectra after adsorption and desorption of 2,6-DTBPy at 423 K for 1 h. Al-MWW showed an intensive band at 3620 cm^{-1} (Fig. 9a), corresponding to acidic bridging hydroxyl groups (Si–OH–Al) in the framework together with the band at 3745 cm^{-1} attributed to external silanol groups [21,55]. The adsorption with 2,6-DTBPy made the 3620 cm^{-1} band almost intact, whereas decreased the intensity of the 3745 cm^{-1} band (Fig. 9b). The amine molecules thus hardly reached the acid sites located within the 10-MR channels of MWW structures, but may interact with the external silanols. The adsorption developed two characteristic bands at 3370 cm^{-1} and 1616 cm^{-1} (Fig. 9c), which are assigned to the N–H stretching vibration in $DTBPyH^+$ and corresponding ring vibration mode [49]. They are taken as the presence of strong Brønsted acid sites on the crystallite surface of Al-MWW. These acid sites were probably generated from those tetrahedral Al ions located in 12-MR side cups. Becoming less intensive, the bands at 3370 and 1616 cm^{-1} were still observed in the spectrum of Al-MWW/B-MWW (Fig. 9c). However, they were invisible for Al-MWW@B-MWW(1.5 g) (Fig. 9d). The adsorption with 2,6-DTBPy only developed several bands at 2897 cm^{-1} and 1700 cm^{-1} due to the amine species physisorbed and/or weakly interacted with the silanols and Si–OH–B groups on the crystallite

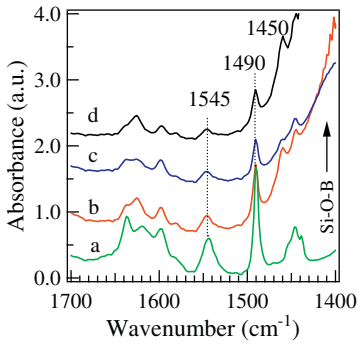

Fig. 8. IR spectra of Al-MWW (a), Al-MWW/B-MWW (b), Al-MWW@B-MWW(1.5 g) (c), and B-MWW(d) after pyridine adsorption and desorption at 423 K for 1 h.

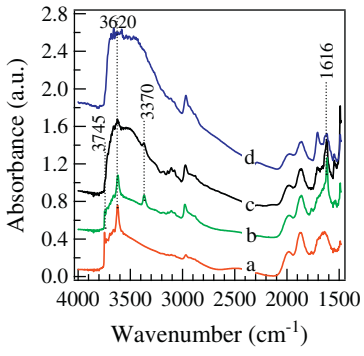

Fig. 9. IR spectra of Al-MWW (a and b), Al-MWW/B-MWW (c), Al-MWW@B-MWW(1.5 g) (d), before (a) and after (b–d) 2,6-di-tert-butyl-pyridine adsorption/desorption at 423 K for 1 h.

surface [49]. Different obviously from the Al-MWW/B-MWW physical mixture, Al-MWW@B-MWW was almost free of strong Brønsted acid sites on the crystallite surface. The overgrowth of B-MWW shell would block efficiently the Al-related acid sites on the external surface of Al-MWW core because B-MWW was of a non-acidic or weakly acidic nature.

3.3. Catalytic properties of Al-MWW@B-MWW in toluene disproportionation

Taking advantage of the core/shell structure of Al-MWW@B-MWW composite, we have tried to achieve shape-selective disproportionation of toluene. Its catalytic properties were compared with those of B-MWW and Al-MWW catalysts. As shown in Scheme 1, the reaction gave benzene and xylene isomers as the main products. Other by-products such as ethylbenzene and C_{9+} aromatics were also formed as a result of trans-alkylation, but their amount was less than 1% in total products. Table 2 summarizes the toluene conversion, molar ratio of benzene/xylene, and fractions of xylene isomers obtained from the toluene disproportionation at 573 K. The benzene/xylene molar ratio was close to unity, indicating a so-called clean disproportionation occurred over all zeolites investigated. The molar fraction of produced *p*-xylene in three xylene isomers is defined as the *para*-selectivity. B-MWW showed an extremely very low toluene conversion (1.4%) because of weak acidity as characterized by NH_3-TPD. Possessing Al-derived strong acid sites, the parent Al-MWW catalyst with the lowest Si/Al ratio was the most active, giving a toluene conversion of 21.8%. Its *para*-selectivity reached 38.6% which exceeded the equilibrium value of xylene isomers (ca. 24%), suggesting that Al-MWW is a potentially shape selective for toluene disproportionation. The fraction of *m*-xylene was the highest among the xylene isomers because it is thermodynamically more stable than the other two isomers. The physical mixture of Al-MWW/B-MWW gave a lower toluene conversion (9.2%) and a higher *p*-xylene selectivity (48.7%) than Al-MWW. Similarly, the overgrowth of B-MWW lowered the toluene conversion for the Al-MWW@B-MWW composites in comparison with Al-MWW. This is simply because Al-MWW@B-MWW and Al-MWW/B-MWW both contained less Al amount and Brønsted acid sites as previously characterized by Py-IR and NH_3-TPD. In terms of specific activity, i.e., turnover frequency (TOF), three kinds of Al-MWW-containing zeolites were comparably active to the reaction. However, the conversion decreased from 18.7% to 5.5% when decreasing the Al-MWW content in Al-MWW@B-MWW from 3 g to 1.5 g, which is probably due to an increase in crystal thickness (Fig. 3b–e) and then a decrease in diffusion rate of reactant molecules. Meanwhile, a significant change in the distribution of xylene isomers was also observed. The selectivity of *p*-xylene increased greatly with decreasing Al-MWW content in the catalyst. Far in excess of the equilibrium value, it reached 89.8% at 5.5% toluene conversion for Al-MWW@B-MWW(1.5 g). On the other hand, the selectivities for *o*- and *m*-xylene decreased simultaneously. Considering that the product selectivity depended on the reaction level, that is, toluene conversion, Al-MWW@B-MWW was obviously more shape selective than Al-MWW/B-MWW. Moreover, Al-MWW@B-MWW(1.5 g) showed stable toluene conversion and *p*-xylene selectivity after the spent catalyst was regenerated by oxygen treatment at 773 K for 1 h and subjected to reuse in the toluene disproportionation (Fig. S1), indicating that the core/shell zeolite was a robust and thermally stable catalyst.

Fig. 10 shows the changes of toluene conversion and *para*-selectivity with time on stream (TOS) for Al-MWW and Al-MWW@B-MWW(1.5 g). Al-MWW exhibited a higher initial activity but deactivated easily with TOS. The conversion of toluene decreased rapidly from 21.8% at 30 min to 1.9% at 180 min. A significant

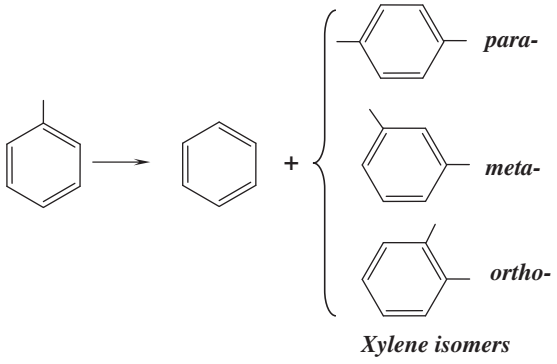

Scheme 1. Distribution of main products in toluene disproportionation.

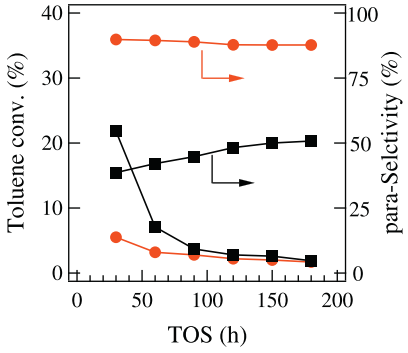

Fig. 10. Toluene disproportionation over Al-MWW (■) and Al-MWW@B-MWW(1.5 g) (●). Reaction conditions: see Table 2.

Table 2
The results of toluene disproportionation over various MWW-type zeolite catalysts.[a]

Catalyst	B-MWW	Al-MWW	Al-MWW/B-MWW	Al-MWW @B-MWW(3 g)	Al-MWW @B-MWW(2.5 g)	Al-MWW @B-MWW(1.5 g)
Si/Al ratio [b]	–	22	65	50	56	64
Si/B ratio [b]	12.6	–	–	115	108	14
Toluene conv. (%)	1.4	21.8	9.2	18.7	8.2	5.5
Benzene/xylene ratio	1.15	1.04	1.05	0.99	1.18	1.02
Fraction in xylene (%)						
p-Xylene	26.0	38.6	48.7	46.6	53.6	89.8
m-Xylene	49.0	52.5	46.9	50.5	44.6	9.4
o-Xylene	25.0	8.9	4.4	2.9	1.8	0.8
TOF (h^{-1}) [c]	–	23	27	28	24	17

[a] Reaction conditions: cat., 0.2 g; temp., 573 K; toluene feed, 1.7 mL h^{-1}; N_2, 30 mL min^{-1}; TOS, 0.5 h.
[b] Obtained by ICP.
[c] Obtained by dividing the molar amount of converted toluene with TOS of 0.5 h with that of aluminum in the catalyst.

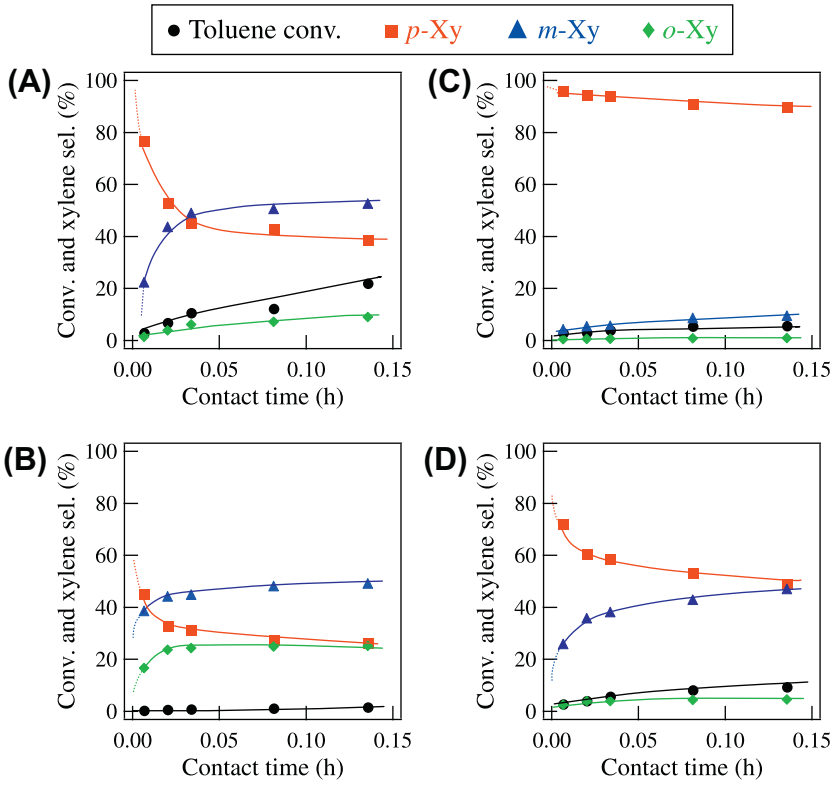

Fig. 11. Change in toluene conversion and fractions of xylene isomers with W/F in toluene disproportionation over Al-MWW (A), B-MWW (B), Al-MWW@B-MWW(1.5 g) (C), and Al-MWW/B-MWW (D). Reaction conditions: catalyst, 0.01–0.2 g; others, see Table 2.

deactivation has also been reported over ZSM-5 and ZSM-22 [56], which is suggested to be a feature typical of medium pore zeolites. The decrease in toluene conversion was mostly caused by coke deposition as the color of the catalyst changed from white to black during reaction course. We have demonstrated that the activity was resorted readily when the deactivated catalyst was regenerated by combustion in air at 773 K [32], implying that this kind of deactivation is reversible. On the other hand, the *para*-selectivity increased slightly with prolonging TOS, reaching 50.8% at 180 min. The coke formation seemed to retard the isomerization of *p*-xylene as well. In comparison with Al-MWW, different catalytic behaviors were observed for Al-MWW@B-MWW(1.5 g), which showed a much lower toluene conversion because of a lower aluminosilicate content. The dilution and covering with B-MWW partially inhibited the coke formation, which moderated the deactivation rate. On the other hand, Al-MWW@B-MWW showed a higher and stable *para*-selectivity (>88%) independent of TOS and toluene conversion.

The enhancement of *para*-selectivity and reduction of deactivation rate observed for Al-MWW@B-MWW implied that it was intrinsically different from Al-MWW in terms of shape-selective disproportionation. Since the *para*-selectivity depended closely on the toluene conversion level and reaction time in particular for Al-MWW, the contact time (the reciprocal of WHSV) was thus varied in a wide range to determine which xylene isomer was primarily produced. Table S1 shows the detailed catalytic data obtained by varying the catalyst amount, while Fig. 11 illustrates the dependence of toluene conversion and xylene distributions on the contact time. The reactions were carried out at 573 K for all samples by varying the catalyst amount while fixing the feed rate of toluene and carrier gas flow. The toluene conversion decreased reasonably with decreasing contact time for all samples. In the case of Al-MWW, the *para*-selectivity increased greatly with decreasing contact time, while the fractions of *o*- and *m*-xylenes both decreased and approached almost to zero (Fig. 11A). The results indicated that *p*-xylene was the primary product in toluene disproportionation on Al-MWW. *p*-Xylene initially produced was possibly isomerized to *o*- and *m*-isomers when reaching the acid sites in next catalyst bed especially at a prolonged contact time. However, Al-MWW@B-MWW(1.5 g) showed a much higher *para*-selectivity and almost no *o*-xylene formation (Fig. 11B). The variation of W/F did not result in significant changes of the fractions of xylene isomers. Al-MWW@B-MWW was still characteristic of producing *p*-xylene as the primary product, but it became a more shape-selective catalyst than conventional Al-MWW. The catalytic nature of Al-MWW@B-MWW also differed from that of B-MWW and Al-MWW/B-MWW. With only weak acid sites, B-MWW was almost inactive for toluene disproportionation, giving xylene isomer distributions not worth discussing (Fig. 11C). The physical mixture, Al-MWW/B-MWW, showed an improved *para*-selectivity in comparison with Al-MWW (Fig. 11D). However, the *para*-selectivity was much lower than that of Al-MWW@B-MWW and decreased with prolonging contact time. Thus, different from orientated crystal overgrowth in Al-MWW@B-MWW, the physical dilution with B-MWW of weak acidity did alter the fundamental shape selectivity of Al-MWW.

Since the product selectivity was dependent of reaction level, the reactions were then carried out at various contact times to investigate effect of toluene conversion on *para*-selectivity. Fig. 12 shows the *para*-selectivity as a function of toluene conversion. Over parent Al-MWW, the *para*-selectivity decreased monotonously with the toluene conversion. At the highest toluene conversion of 21.8%, the *p*-xylene selectivity was only 38.6% (Fig. 12a), slightly higher than the equilibrium value. The *p*-xylene selectivity of Al-MWW/B-MWW was slightly higher than Al-MWW, but the shape-selective property of Al-MWW was

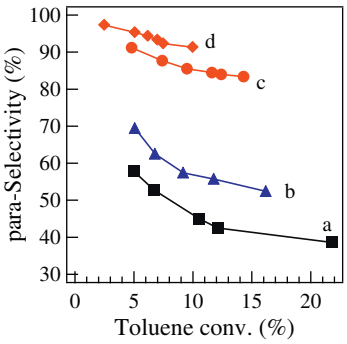

Fig. 12. Dependence of *para*-selectivity on toluene conversion over Al-MWW (a), Al-MWW/B-MWW (b), Al-MWW@B-MWW(1.5 g) (c), and acid-treated Al-MWW@B-MWW(1.5 g) (d). The acid treatment was carried out using 6 M HNO_3 at 373 K for 10 h, followed by calcination in air for 10 h at 973 K. Reaction conditions: cat., 0.01–0.35 g; others, see Table 2.

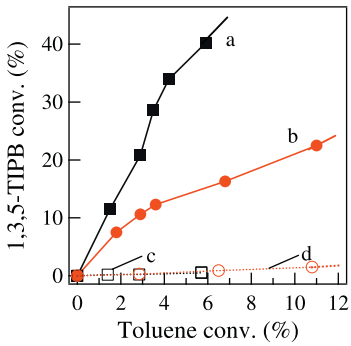

Fig. 13. The correlation between 1,3,5-TIPB cracking and toluene disproportionation over Al-MWW (a and c) and Al-MWW@B-MWW(1.5 g) (b and d) without (a and b) or with (c and d) the presence of 2,4-DMQ. Toluene disproportionation and 1,3,5-TIPB cracking conditions: cat., 0.01–0.25 g; others, see Table 2; 2,4-DMQ feeding rate, 100 μmin^{-1} (if added).

unchanged after physical dilution (Fig. 12b). However, Al-MWW@B-MWW(1.5 g) showed greatly enhanced *para*-selectivity which was less dependent of toluene conversion (Fig. 12c). The core/shell-structured materials were thus characterized by a high shape selectivity. The observation was fully in agreement with the results previously reported on ZSM-5@silicalite-1 which showed a high *para*-selective in toluene methylation as a result of removing the surface acidity available for isomerization [41,42].

Disproportionation of toluene is referred as an electrophilic substitution reaction via a two-molecule intermediate [57,58]. The bulky intermediate favored *para*-orientation within 10-MR micropores of zeolites. This kind of "transition state shape selectivity" would produce *p*-xylene as the primary product. Nevertheless, subsequent isomerization of *p*-xylene to *m*- and *o*-isomers would make the isomer distributions approach to thermodynamic equilibrium. The isomerization occurred easily at a prolonged contact time in particular on non-selective acid sites on the external surface or near pore entrance. The isomerization of *p*-xylene was once reported to take place easily on the Brønsted acid sites of MCM-22 [32,59]. Similar results were observed during the disproportionation of toluene over ZSM-5 [60]. In the case of CLD modifications of ZSM-5 [20,21], the *para*-selectivity increased remarkably only when the acid sites on the external surface were passivated extensively, or the pore mouth regions were finely modified by approximately 95% with silica layer deposition. Similarly, the acid sites on the external surface of premade Al-MWW were covered and passivated by isomorphic overgrowth of borosilicate with an extremely weak acidity as characterized by 2,6-DTBPy-IR spectra (Fig. 9). This would suppress effectively the isomerization of *p*-xylene and then improve the *para*-selectivity significantly. Moreover, the *p*-xylene selectivity was further increased and reached 94% when Al-MWW@B-MWW(1.5 g) was refluxed using 6 M HNO_3 (Fig. 12d). The *para*-selectivity was comparable or even superior to those observed at 873 K on the ZSM-5 zeolites modified with phosphorous, MgO, or boron [1,2]. The acid treatment may induce dealumination either in the framework or on the external surface and then reduced the amount of acid sites available for isomerization of *p*-xylene.

The cracking of 1,3,5-triisopropylbenzene (TIPB) has been carried out to investigate the catalytic properties correlated to the zeolite surface before and after secondary growth of B-MWW. With a bulky molecular dimension, TIPB (0.95 nm) is believed not to enter the 10-MR windows of MWW zeolites [61]. Its cracking activity reflects the catalytic behaviors mainly related to the external acid sites. The 1,3,5-TIPB conversion in cracking is plotted against the toluene conversion in disproportionation in Fig. 13. In the presence of 2,4-DMQ, the toluene disproportionation was little influenced, whereas both Al-MWW and Al-MWW@B-MWW became almost inactive for 1,3,5-TIPB cracking (Fig. 13c and d). 2,4-DMQ is a bulky poisoning agent that selectively blocks the active sites on the external surface of zeolite crystallites such as ZSM-5 [62], MCM-22 [32], and Ti-MWW [63]. Above results confirmed that it was reliable for evaluating the surface acidity using 1,3,5-TIPB cracking. Al-MWW and Al-MWW@B-MWW(1.5 g) gave different relationships between two reactions in the absence of 2,4-DMQ. 1,3,5-TIPB conversion was almost proportional to toluene conversion for parent Al-MWW (Fig. 13a). However, the conversion was greatly reduced in the case of the Al-MWW@B-MWW(1.5 g) when compared at the same toluene conversion (Fig. 13b), suggesting that the concentration of active sites on the external surface of Al-MWW@B-MWW was much lower. This was in agreement with previous 2,6-DTBPy adsorption. Therefore, the observed improvement in *para*-selectivity by overgrowing B-MWW shell could be reasonably ascribed to the removal of the acid sites on the external surface, and then the suppression of consequent isomerization of *p*-xylene. *p*-Xylene was the primary product in the toluene disproportionation over MWW-type zeolites (Fig. 11). *p*-Xylene formed inside intracrystal micropores would be isomerized to *m*- and *o*-xylene when it diffused out of the pores and reached on the non-shape-selective acid sites on the external surface.

The *para*-selectivity was improved efficiently by overgrowth B-MWW on Al-MWW, but it still did not reach 100%. There may be other factors governing the *para*-selectivity of Al-MWW. It was reported that the acid sites within the 10-MR channels of MCM-22 could catalyze the isomerization of *p*-xylene at 573 K [32], and the xylene isomerization occurred readily over ZSM-5 with 10-MR channels at low temperatures (473 K) in the order of *p*- > *m*- > *o*-xylene [64]. We thus have investigated the isomerization of *p*-xylene at 573 K and correlated its activity to toluene disproportionation (Fig. S3). The *p*-xylene conversion was almost proportional to the toluene conversion for both Al-MWW and Al-MWW@B-MWW. When compared at the same level of toluene conversion, Al-MWW@B-MWW was only slightly less active than Al-MWW. This difference was much smaller than that observed in the 1,3,5-TIPB cracking mentioned above (Fig. 13). The overgrowth of B-MWW removed selectively the surface acid sites but not those inside the 10-MR pores which still contributed to the isomerization of xylene. This is probably the reason that the *para*-selectivity did not reach 100% even after the acid sites on the external surface were blocked extensively by B-MWW covering.

4. Conclusion

Shape-selective core/shell-structured MWW-type zeolite composites have been prepared successfully through isomorphic overgrowth of borosilicate on premade aluminosilicate crystallites. In comparison with bare crystallites of Al-MWW, the Al-MWW@B-MWW composite catalysts exhibited much higher *p*-xylene selectivity in the disproportionation of toluene. The enhanced *para*-selectivity observed for Al-MWW@B-MWW composite was ascribed to effective suppression of isomerization of *p*-xylene as a result of removal of non-shape-selective acid sites on the external surface. Overgrowing non-acidic or weakly acidic borosilicate on the crystallites of aluminosilicate proves to be novel and convenient technique for design synthesis of shape-selective zeolite catalysts.

Acknowledgments

We gratefully acknowledge the NSFC of China (20890124, 20925310, and 20873043), the Science and Technology Commission of Shanghai Municipality (09XD1401500), and the Shanghai Leading Academic Discipline Project (B409).

Appendix A. Supplementary material

Supplementary data associated with this article can be found, in the online version, at doi:10.1016/j.jcat.2011.08.007.

References

[1] N.Y. Chen, W.W. Kaeding, F.G. Dwyer, J. Am. Chem. Soc. 101 (1979) 6783.
[2] W.W. Kaeding, C. Chu, L.B. Young, B. Weinstein, S.A. Butter, J. Catal. 67 (1981) 159.
[3] M.A. Uguina, J.L. Sotelo, D.P. Serrano, Appl. Catal. A 76 (1991) 183.
[4] G. Mirth, J. Čejka, J.A. Lercher, J. Catal. 139 (1993) 24.
[5] G. Mirth, J.A. Lercher, J. Catal. 147 (1994) 199.
[6] J. Čejka, N. Žilková, B. Wichterlova, G. Elder-Mirth, J.A. Lercher, Zeolites 17 (1996) 265.
[7] R. Mantha, S. Bhatia, M.S. Rao, Ind. Eng. Chem. Res. 30 (1991) 281.
[8] T. Yashima, H. Ahmad, K. Yamazaki, M. Katsuta, N. Hara, J. Catal. 16 (1970) 273.
[9] T. Yashima, K. Sato, T. Hayasaka, N. Hara, J. Catal. 26 (1972) 303.
[10] A.E. Palomares, G. Elder-Mirth, J.A. Lercher, J. Catal. 168 (1997) 442.
[11] E. Dumitriu, V. Hulea, S. Kaliaguine, M.M. Huang, Appl. Catal. A 135 (1996) 57.
[12] P. Ratnasarmy, R.N. Bhat, S.K. Pokhriyal, J. Catal. 119 (1989) 65.
[13] J. Das, Y.S. Bhat, A.B. Halgeri, Catal. Lett. 23 (1994) 161.
[14] S. Zheng, H.R. Heydenrych, A. Jentys, J.A. Lercher, J. Phys. Chem. B 106 (2002) 9552.
[15] J. Čejka, A. Krejčí, N. Žilková, J. Kotrla, S. Ernst, A. Weber, Micropor. Mesopor. Mater. 53 (2002) 121.
[16] F. Bauer, W.H. Chen, Q. Zhao, A. Freyer, S.B. Liu, Micropor. Mesopor. Mater. 47 (2001) 67.
[17] F. Bauer, W.H. Chen, E. Bilz, A. Freyer, V. Sauerland, S.B. Liu, J. Catal. 251 (2007) 258.
[18] J.H. Kim, A. Ishida, M. Okajima, M. Niwa, J. Catal. 161 (1996) 387.
[19] A.B. Halgeri, J. Das, Catal. Today 73 (2002) 65.
[20] S. Zheng, H. Tanaka, A. Jentys, J.A. Lercher, J. Phys. Chem. B 108 (2004) 1337.
[21] S. Laforge, D. Martin, J.L. Paillaud, M. Gusinet, J. Catal. 220 (2003) 92.
[22] M.K. Rubin, P. Chu, US Patent 4,954,325, 1990.
[23] L. Puppe, J. Weisser, US Patent 4,439,409, 1984.
[24] S.I. Zones, D.I. Holtermann, R.A. Innes, T.A. Pecoraro, D.S. Santilli, J.N. Ziemer, US Patent 4,826,667, 1989.
[25] G. Bellussi, G. Perego, M.G. Clerici, A. Giusti, European Patent Application 293,032, 1988.
[26] M.A. Camblor, A. Corma, M.-J. Díaz-Cabañas, Ch. Baerlocher, J. Phys. Chem. B 102 (1998) 44.
[27] S.L. Lawton, M.E. Leonowicz, R.D. Partridge, P. Chen, M.K. Rubin, Micropor. Mesopor. Mater. 23 (1998) 109.
[28] C. Perego, S. Amarilli, R. Millini, G. Bellussi, G. Girotti, G. Terzoni, Micropor. Mater. 6 (1996) 395.
[29] A. Corma, V. Martynez-Soria, E. Schnoeveld, J. Catal. 192 (2000) 163.
[30] Zeolites for Cleaner Technologies, Catalytic Science Series, vol. 3, Imperial College Press, London, 2002, p. 223.
[31] Z. Zhu, Q. Chen, W. Zhu, D. Kong, C. Li, Catal. Today 321 (2004) 93.
[32] P. Wu, T. Komatsu, T. Yashima, Micropor. Mesopor. Mater. 22 (1998) 343.
[33] S.-H. Park, H.-K. Rhee, React. Kinet. Catal. Lett. 78 (2003) 73.
[34] P. Prokesova, N. Žilková, S. Mintova, T. Bein, J. Čejka, Appl. Catal. A 281 (2005) 85.
[35] P. Prokesova, S. Mintova, J. Čejka, T. Bein, Mater. Sci. Eng. C 23 (2003) 1001.
[36] F. Zhou, X. Li, A.J. Wang, L.Y. Wang, X.D. Yang, Y.K. Hu, Catal. Today 150 (2010) 218.
[37] H.Y. Xu, J.Q. Guan, S.J. Wu, Q.B. Kan, J. Colloid Interface Sci. 329 (2009) 346.
[38] P. Prokesova, S. Mintova, J. Čejka, T. Bein, Micropor. Mesopor. Mater. 64 (2003) 165.
[39] L.D. Rollman, US Patent 4,088,605, 1978.
[40] N. Nishiyama, M. Miyamoto, T. Kamei, Y. Egashira, K. Ueyama, Stud. Surf. Sci. Catal. 162 (2006) 275.
[41] D.V. Vu, M. Miyamoto, N. Nishiyama, Y. Egashira, K. Ueyama, J. Catal. 243 (2006) 389.
[42] M. Miyamoto, T. Kamei, N. Nishiyama, Y. Egashira, K. Ueyama, Adv. Mater. 17 (2005) 1985.
[43] Y. Bouizi, L. Rouleau, V.P. Valtchev, Chem. Mater. 18 (2006) 4959.
[44] Q. Li, W. Zheng, J. Hedlund, D. Creaser, H. Zhang, X. Zou, A.J. Bons, Micropor. Mesopor. Mater. 78 (2005) 1.
[45] W. Vermeiren, J.P. Dath, V. Buono, DE Patent 1,661,859, 2006.
[46] B. Xue, J. Xu, C.F. Xu, R.Z. Wu, Y.X. Li, K. Zhang, Catal. Commun. 12 (2010) 95.
[47] M.A. Camblor, C. Corell, A. Corma, M.-J. Díaz-Cabañas, S. Nicolopoulos, J.M. Gonzalez-Calbet, M. Vallet-Regi, Chem. Mater. 8 (1996) 2415.
[48] A. Corma, V. Fornés, L. Forni, F. Márquez, J. Martínez-Triguero, D. Moscotti, J. Catal. 179 (1998) 451.
[49] A. Ungureanu, T.V. Hoang, D. Trong On, E. Dumitriu, S. Kaliaguine, Appl. Catal. A 294 (2005) 92.
[50] J. Roeseler, G.P. Heitmann, W.F. Hölderich, Appl. Catal. A 144 (1996) 319.
[51] Y.C. Shang, P.P. Yang, M.J. Jia, W.X. Zhang, T.H. Wu, Catal. Commun. 9 (2008) 907.
[52] B. Xue, Y.X. Li, L.J. Deng, Catal. Commun. 10 (2009) 1609.
[53] J. Datka, B. Gil, J. Zlamaniec, P. Batamack, J. Fraissard, P. Massiani, Polish J. Chem. 73 (1999) 535.
[54] P. Wu, T. Tatsumi, T. Komatsu, T. Yashima, J. Catal. 202 (2001) 245.
[55] J.P. Marques, I. Gener, P. Ayrault, J.C. Bordado, J.M. Lopes, F.R. Ribeiro, M. Guisnet, Micropor. Mesopor. Mater. 60 (2003) 251.
[56] I.V. Mishin, H.K. Beyer, H.G. Karge, Appl. Catal. A 180 (1999) 207.
[57] H.A. Benesi, J. Catal. 8 (1967) 368.
[58] K.M. Wang, J.H. Lunsford, J. Catal. 24 (1972) 262.
[59] Y.G. Li, W.X. Xie, S. Yong, Appl. Catal. A 150 (1997) 231.
[60] J.-H. Kim, S. Namba, T. Yashima, Appl. Catal. A 83 (1992) 51.
[61] Zh.X. Qin, B.J. Shen, X.H. Gao, F. Lin, B.J. Wang, Ch.M. Xu, J. Catal. 278 (2011) 266.
[62] S. Namba, S. Nakanishi, T. Yashima, J. Catal. 88 (1984) 505.
[63] Y. Wang, Y.M. Liu, L.L. Wang, H.H. Wu, X.H. Li, M.Y. He, P. Wu, J. Phys. Chem. C 113 (2009) 18753.
[64] L.B. Young, S.A. Butter, W.W. Kaeding, J. Catal. 76 (1982) 418.